Journal of Power Sources 239 (2013) 269–276

Contents lists available at SciVerse ScienceDirect

Journal of Power Sources

journal homepage: www.elsevier.com/locate/jpowsour

Effect of solid electrolyte interface (SEI) film on cyclic performance of $Li_4Ti_5O_{12}$ anodes for Li ion batteries

Yan-Bing He [a], Ming Liu [b], Zhen-Dong Huang [a], Biao Zhang [a], Yang Yu [a], Baohua Li [b], Feiyu Kang [b], Jang-Kyo Kim [a,*]

[a] Department of Mechanical Engineering, Hong Kong University of Science and Technology, Clear Water Bay, Kowloon, Hong Kong
[b] Key Laboratory of Thermal Management Engineering and Materials, Graduate School at Shenzhen, Tsinghua University, Shenzhen 518055, China

HIGHLIGHTS

- An SEI film can be formed on the surface of $Li_4Ti_5O_{12}$ anode even above 1 V.
- The formation of SEI film is much affected by the morphology of the electrode.
- It is assumed that the SEI film has a significant effect on cyclic performance of $Li_4Ti_5O_{12}$ electrode.
- It is found that vinylene carbonate (VC) helps rapid formation of a protective SEI film on $Li_4Ti_5O_{12}$.

ARTICLE INFO

Article history:
Received 20 February 2013
Received in revised form
24 March 2013
Accepted 25 March 2013
Available online 5 April 2013

Keywords:
Lithium titanate
Solid electrolyte interface
Surface morphology
Vinylene carbonate

ABSTRACT

Understanding the formation of SEI films on $Li_4Ti_5O_{12}$ (LTO) anodes offers a major benefit to large-scale applications of lithium ion batteries made therefrom. This paper reveals that an SEI film is formed above 1 V due to the interfacial reaction between the electrode and electrolyte: LTO anodes are previously considered free from SEI films when cycled between 1 and 3 V. The reactivity and the formation of SEI films are much affected by the morphology and surface area of the electrode. To study the above, LTO powders with different morphologies are synthesized using lithium acetate (LA) and lithium hydroxide (LH) as the lithium sources. LTO–LH consisting of agglomerates of primary small particles with a large surface area has higher reactivity than LTO–LA with a cubic structure and small surface area. As a result, the LTO–LH anode with a smooth SEI film offers better cyclic performance than the LTO–LA anode with a porous SEI film. The addition of vinylene carbonate to the electrolyte facilitates rapid formation of a protective SEI film on LTO–LA, greatly improving the rate and cyclic performance: stable specific capacity of 155.6 mAh g^{-1} and remarkable 135.2 mAh g^{-1} after 500 cycles at 10 C are recorded.

© 2013 Elsevier B.V. All rights reserved.

1. Introduction

Spinel $Li_4Ti_5O_{12}$ (LTO) has a theoretical capacity of 175 mAh g^{-1} and exhibits excellent reversibility due to its zero volume change during charge/discharge cycles. LTO also demonstrates excellent thermal stability and cyclic performance, making it a potential anode material for high power applications [1–3]. Nevertheless, LTO suffers from a low intrinsic electronic conductivity and lithium-ion diffusion coefficient [4,5], resulting in poor high-rate capacities. Extensive studies have hitherto been carried out to address these issues and different material modifications have been proposed with varied success, including carbon coating [6–9], metal and non-metal ion doping [5,10–13], hybridization with carbon and metal powders [14–19], reduction in LTO particle size [20], etc. In addition, various nanostructured $Li_4Ti_5O_{12}$, such as hollow microspheres [21], flower-like nanosheets [22], sawtooth-like nanosheets [23], hierarchical structures [24] and rutile-TiO_2 nanocoatings [4], have been prepared using lithium hydroxide as the lithium source based on the hydrothermal method. They all presented high rate charge/discharge performance due to the large surface area required for reactions with the electrolyte. Nevertheless, these electrode materials often showed low tap densities and high irreversible capacity losses.

Another important reason behind the use of LTO as a potential anode material for high power lithium ion batteries (LIBs) is that LTO is considered free from SEI films and therefore is much safer and more stable than carbon-based materials. LTO

* Corresponding author. Tel.: +852 2358 7207; fax: +852 2358 1543.
E-mail address: mejkkim@ust.hk (J.-K. Kim).

0378-7753/$ – see front matter © 2013 Elsevier B.V. All rights reserved.
http://dx.doi.org/10.1016/j.jpowsour.2013.03.141

has a stable voltage plateau at approximately 1.5 V versus Li^+/Li and its end discharge potential is usually 1 V, both of which are above the potential range where most electrolyte materials or solvents are reduced [25–27]. This means that the reduction of electrolyte on the surface of LTO can be effectively avoided due to the favorable potential difference. However, this fact is often incorrectly understood that an SEI film cannot be formed on the LTO surface.

It is well-known that a protective SEI film has to be formed to suppress the further decomposition process of electrolyte solution and protect the carbon anode. The formation mechanisms and the properties of SEI films on a carbon anode are of paramount importance in view of their influences on electrochemical and safety performance of LIBs [28,29]. Commercial LIBs, therefore, are allowed to form an SEI film on carbon anode at a low current during the initial several charge/discharge cycles. The mechanisms involved in the film formation are known to be affected by the applied voltage, current, temperature and the type of solvent used [30–33]. In addition, the reduction products of electrolyte solution – a main component of SEI films – are easily decomposed to react with the electrolyte solution at high temperatures [34]. The high thermal reactivity of the lithiated graphite anodes with the electrolyte solution means that the carbon materials used as the dominant source of anodes for current LIBs do not have high safety performance [35,36].

It is previously misunderstood that an SEI film cannot be formed on the surface of LTO electrodes when cycled above 1 V because the electrolyte solution can only be reduced below 1 V. As such, the formation of SEI films has been neglected with little attention so far. However, we demonstrated in this study that an SEI film could also be formed on the surface of LTO electrodes when cycled at 1–3 V. The interfacial reaction between LTO and the electrolyte solution was responsible for the observation, greatly affected by the morphology of LTO powders. The formation mechanisms and the role of the SEI films during the cyclic tests were successfully identified. Particular emphasis was placed on evaluating the effects of SEI films on the rate and cyclic performance of LTO electrodes. For this purpose, a facile hydrothermal method was employed to prepare LTO particles using cetyltrimethylammonium bromide (CTAB) as a surfactant to control the hydrolysis rate of tetrabutyl titanate ($Ti(OC_4H_9)_4$). To specifically evaluate the reactivity and the formation of SEI films, LTO powders with different morphologies were prepared using lithium acetate (LA) and lithium hydroxide (LH) as the lithium source.

2. Experimental

2.1. Synthesis of LTO–LA and LTO–LH

CTAB was used as a surfactant in the hydrolysis process. 0.39 g CTAB was dissolved into 20 mL deionized water at room temperature, and 5 mL $Ti(OC_4H_9)_4$ was introduced stepwisely into the CTAB solution under magnetic stirring for 3 h to obtain a turbid liquid. It was observed that the $Ti(OC_4H_9)_4$ drop was instantly surrounded by CTA^+ cations, which in turn reduced the contact between $Ti(OC_4H_9)_4$ and water to effectively control the hydrolysis rate before forming $Ti(OH)_4$. 1.259 g lithium acetate dihydrate ($CH_3COOLi\cdot 2H_2O$) was dissolved in 10 mL purified water and the lithium acetate solution was added to the above suspension. The mixture was transferred to a 60 mL Teflon-lined stainless steel autoclave and maintained at 180 °C for 24 h. White precipitate was obtained after the hydrothermal treatment. After drying in an oven at 85 °C, the as-prepared product was calcined at 700 °C for 7 h in air to obtain LTO powders, which are designated as LTO–LA. For comparison, LTO–LH was also prepared using the other lithium source.

2.2. Characterization of structure and morphology of LTO powders

The phase structure of the LTO powders were characterized by X-ray diffraction measurement (XRD, Rigaku D/max 2500/PC using CuKα radiation with $\lambda = 1.5418$ Å). Their morphologies were examined on a field emission scanning electron microscope (FE-SEM, HITACH S4800) at 10 kV and a field emission transmission electron microscope (FE-TEM, JEOL 2010F) at an accelerating voltage of 200 kV. Nitrogen adsorption/desorption isotherms were obtained at 77 K using an automated adsorption apparatus (Micromerit-ics ASAP 2020). The surface area was calculated based on the Brunauer–Emmett–Teller (BET) equation.

2.3. Electrochemical characterization

CR2032-type coin cells were assembled to evaluate the electrochemical performance and SEI film formation on the surface of LTO electrodes. The coin cells consisted of LTO powders as the cathode material, lithium foil as the anode, and polypropylene (Celgard 2500, Celgard Inc., USA) as the separator. The cathode consisted of 80 wt.% LTO, 10 wt.% Super-P carbon black and 10 wt.% poly(vinylidene fluoride) (PVDF) binder to form an active material of about 3.5 mg cm^{-2} with a thickness of about 45 μm, excluding the copper current collector. 1 M $LiPF_6$ in a mixture of ethylene carbonate, dimethyl carbonate and ethylmethyl carbonate (volume ratio: 1:1:1) (1 M $LiPF_6$/EC + DMC + EMC, supplied by Guangzhou Tinci Materials Technology Co. with a moisture content 4.4 ppm and an HF content 15.8 ppm) was used as the electrolyte solution. The cells were assembled in a glove box (Mbraum) filled with high purity argon gas. The assembled cells were cycled at different charge/discharge rates between 0–3 or 1–3 V (Land 2001A Battery Testing System) at room temperature. The cyclic voltammograms (CVs) of LTO electrodes were obtained on an electrochemical working station of VMP3 (Bio Logic Science Instruments) at a scanning rate of 0.1 mV s^{-1} using the LTO electrode as the working electrode, and the lithium foil both as the reference and counter electrodes. The corresponding electrochemical impedance spectra (EIS) were obtained using an electric IM6ex impedance analyzer at a frequency range of $10^{-2} \sim 10^5$ Hz and at a half state of charge by applying a 5 mV ac oscillation.

The coin cells after designated cyclic tests were fully charged before they were disassembled in the glove box for examination. The LTO electrode was rinsed using dimethyl carbonate (DMC) to remove the electrolyte from the electrode surface, and was dried to remove the residual DMC. The surface morphology of the electrode was examined on FE-SEM and FE-TEM, and their elemental compositions were analyzed using X-ray photoelectron spectroscopy (XPS, VGMicro Tech). The C 1s peak for the graphitic carbon at 285 eV was used as a reference for the calibration of XPS peaks. Fourier transform infrared spectroscopy (FTIR, Bio-rad FTS 6000) was used to evaluate the structure of SEI films in the near infrared (NIR) region (600–2000 cm^{-1}).

3. Results and discussion

The XRD patterns of both LTO–LA and LTO–LH powders were in good agreement with the JCPDS standard (card No. 49-0207) and can be indexed to the spinel structure of LTO with the space group *Fd*3*m* (Fig. 1a). Weak diffraction peaks of rutile TiO_2 were detected in LTO–LH, indicating an existence of small fraction of rutile TiO_2 surface layer (see Fig. S1), which was shown to improve the rate performance of LTO [4]. LTO powders prepared using

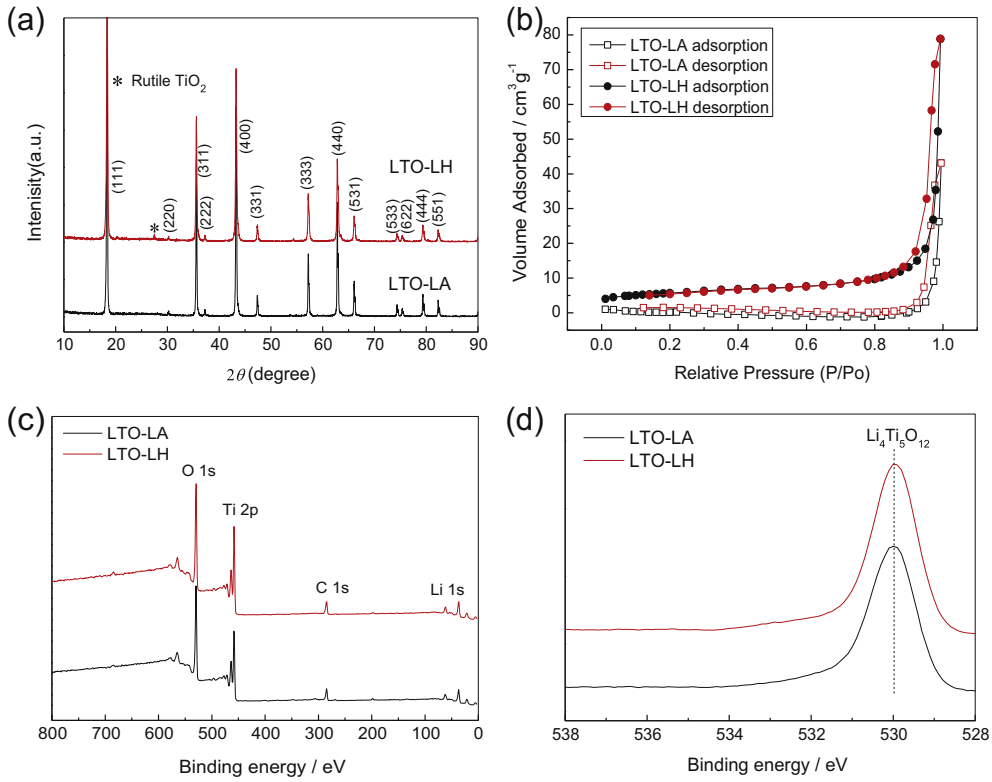


Fig. 1. XRD patterns (a), nitrogen adsorption/desorption isotherms at 77 K (b), XPS survey spectra (c) and high resolution XPS spectra of O 1s (d) of LTO–LA and LTO–LH powders.

different lithium sources presented distinct morphologies and dimensions (Fig. 2a, b). The LTO–LA powder had a cubic structure with a particle size ~200 nm, while the LTO–LH powder was composed of both individual particles of size ~300 nm and agglomerates consisting of much smaller primary particles of size ~30 nm. Using the nitrogen adsorption/desorption isotherms (Fig. 1b), the specific surface area of LTO–LA was measured 0.41 $m^2 g^{-1}$, which is much smaller than 19.93 $m^2 g^{-1}$ for LTO–LH.

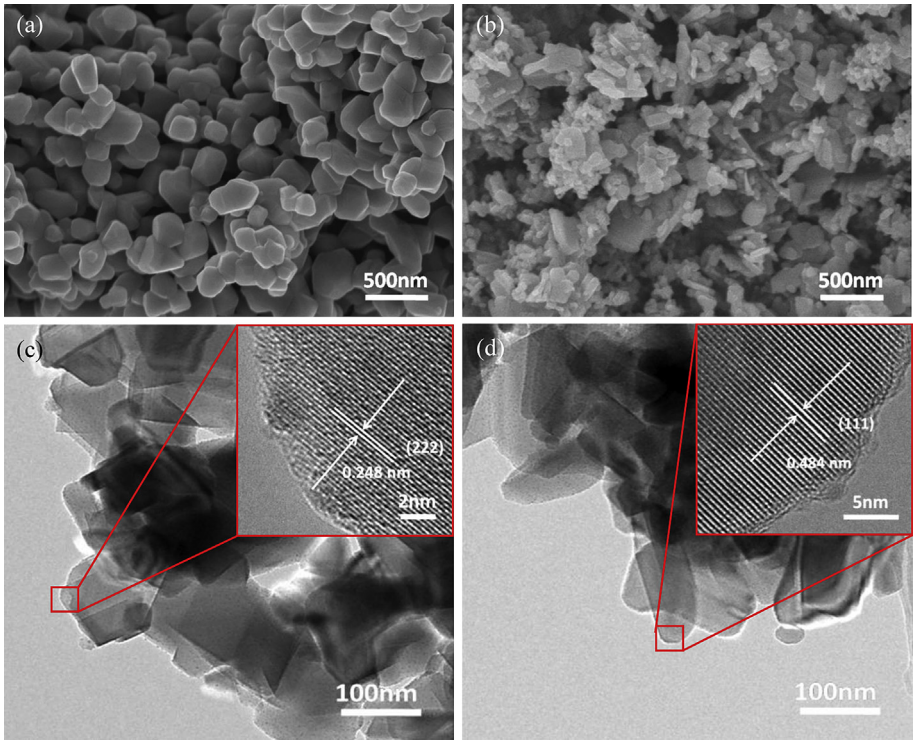


Fig. 2. SEM and TEM images of (a, c) LTO–LA and (b, d) LTO–LH powders.

These observations indicate that the lithium source played an important role in determining the morphologies of the LTO powders with largely different surface areas.

HRTEM images indicate that both LTO–LA and LTO–LH had a well-defined crystal structure (Fig. 2c, d). The *d*-spacing 0.248 nm of the LTO–LA particle is in agreement with that of the (222) plane of spinel LTO, whereas the *d*-spacing 0.484 nm of the LTO–LH particle matches well with that of the (111) plane of spinel LTO. The corresponding XPS survey spectra suggest that the two electrode materials consisted of Ti, O and Li (Fig. 1c). The high-resolution XPS spectra of O 1s displayed a prominent peak at 529.9 eV, consistent with the O^{2-} ions of $Li_4Ti_5O_{12}$ (Fig. 1d). Other O 1s peaks at higher binding energies assigned to functional groups were not found. In summary, both LTO–LA and LTO–LH powders presented a similar surface chemistry and were free from functional groups although they had largely different morphologies.

Fig. 3 shows the electrochemical test results of the LTO–LA and LTO–LH electrodes. The discharge specific capacities of LTO–LA measured at 0.1, 0.5, 1, 5, and 10 C between 1 and 3 V were 174.8, 166.3, 162.3, 151.2 and 139.7 mAh g^{-1}, respectively (Fig. 3a). The capacity at a low rate of 0.1 C was very close to the theoretical capacity of LTO, namely 175 mAh g^{-1}, and the capacity measured at a high rate of 10 C was 79.9% of the value corresponding to 0.1 C. The corresponding capacities of LTO–LH were 173.9, 156.3, 153.2, 148.6 and 144.9 mAh g^{-1}, respectively, which can be regarded equally excellent, especially at high current densities. Testing at 0.5 C after cyclic loading at gradually increasing rates also confirmed the original capacities for both electrode materials.

Moreover, it is interesting to note from Fig. 3a that these two electrodes presented much different cyclic performance depending on the current densities applied. For example, the LTO–LA electrode exhibited more stable initial cyclic performance at 0.1 C than the LTO–LH electrode, and vice versa for longer cycles at a higher current density. The long-term cyclic performance measured both at 1 C and 10 C was generally better for the LTO–LH electrode than the LTO–LA counterpart. The above observations suggest that the cyclic performance of LTO was highly dependent on the morphology of the electrode. It is also worth noting that the lithiation and delithiation potential difference of LTO–LH at 10 C was 0.471 V, which was larger than 0.419 V of LTO–LA (Fig. 3c, d).

The CVs obtained at a scanning rate of 0.1 mV s^{-1} are shown in Fig. 4. Both electrode materials had two sharp, symmetrical redox peaks at 1.46 and 1.67 V (Fig. S2), corresponding to lithium ion insertion/extraction to and from the LTO structure. The peak current densities of the LTO–LA electrode were generally higher than those of the LTO–LH electrode as a consequence of less significant lithiation/delithiation polarization of the former electrode. This can also explain the larger lithiation/delithiation potential differences of the latter electrode at 10 C. It is noted that the peak current density of LTO–LH gradually decreased with increasing cycles, while LTO–LA presented relatively stable CV performance. This behavior was functionally consistent with the initial cyclic performance of the two electrodes when measured at 0.1 C (Fig. 3a), which may be associated with their different morphologies and surface areas. It is seen that the LTO–LH electrode with a larger surface area should have a more active interfacial reaction with the electrolyte solution during the CV test. Part of the capacity was consumed to form the initial SEI film resulting in a high irreversible capacity, which in turn suppressed the further interfacial reaction and decreased the peak current density. In contrast, the interfacial

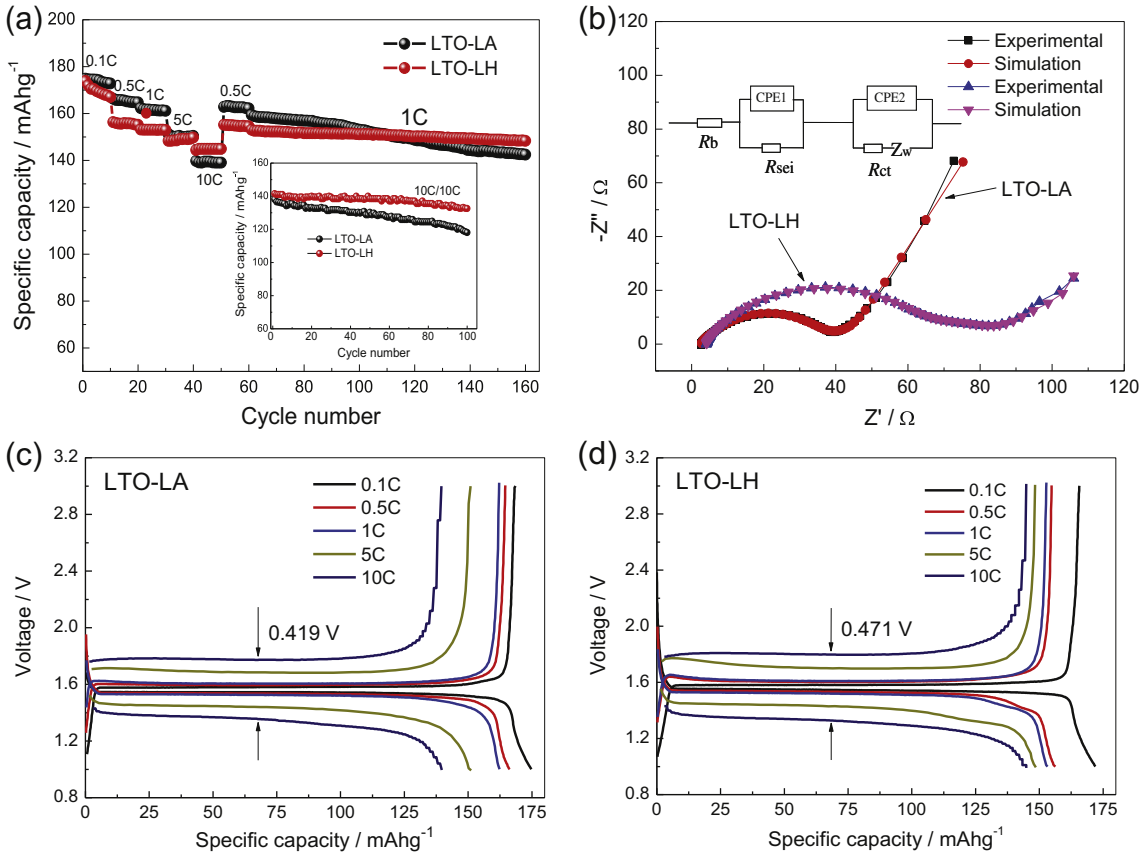


Fig. 3. Electrochemical performance of LTO–LA and LTO–LH electrodes cycled between 1 and 3 V: (a) cyclic performance; (b) experimental and simulation EIS after 3 cycles; (c, d) charge/discharge curves at different rates.

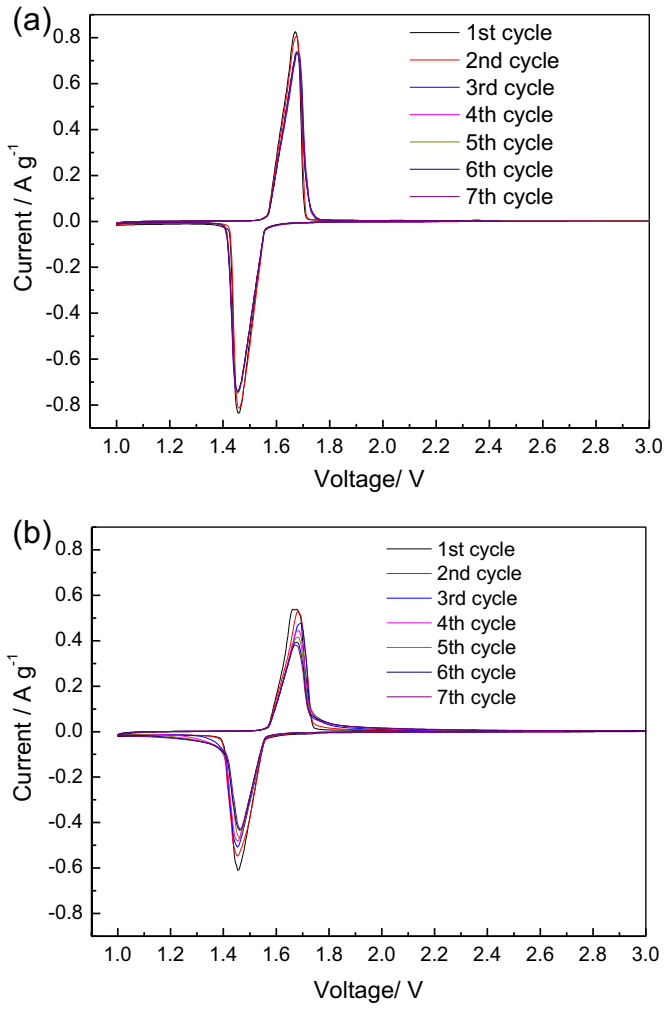


Fig. 4. CV profiles of (a) LTO–LA and (b) LTO–LH electrodes.

reactivity of the LTO–LA electrode was much lower, hence the capacity was mostly used for lithiation of the electrode, giving rise to stable CVs and initial cyclic performance.

To identify the formation of an SEI film between 1 and 3 V, the EIS spectra of both electrodes were also obtained after 3 cycles at 0.1 C (Fig. 3b) along with the simulation results obtained using a Z-view software and the same equivalent circuit. The resistance parameters used in the calculation are given in Table 1. According to the equivalent circuit, the intersection of the EIS diagram with the real axis refers to the bulk resistance (R_b), which reflects the electronic and ionic resistance of two electrodes and electrolyte/separator. The two depressed semicircles observed at high and mid frequencies are attributed to the resistance (R_{sei}) and constant phase elements (CPE1) of the SEI film, and the charge-transfer resistance (R_{ct}) and constant phase elements (CPE2) of the electrode, respectively. Instead of using the capacitance (C_{sei}) of SEI films and double-layer capacitance (C_{dl}) of electrodes, CPE1 and CPE2 were used to take into account the roughness of the LTO electrode surface. The slope line at low frequencies corresponds to the Warburg impedance (Z_w), which is related to lithium ion diffusion within the particles [37–40].

Table 1
Resistance parameters of R_b, R_{sei} and R_{ct} obtained from simulation data in Fig. 3b.

Materials	R_b (Ω)	R_{sei} (Ω)	R_{ct} (Ω)
LTO–LA	2.7	2.4	30.3
LTO–LH	3.9	62.3	18.5

The experimental and simulated EIS curves were almost identical for all conditions studied, indicative of properly chosen equivalent circuit and the corresponding parameters. The spectra for the LTO–LA electrode when cycled 3 times between 1 and 3 V presented only one depressed semicircle at mid- to high frequencies and a slope line at low frequencies, whereas it showed two partially overlapped and depressed semicircles at mid- to high frequencies and a slope line at low frequencies for the LTO–LH electrode cycled under the same condition (Fig. 3b). This observation verified the formation of an SEI film on the surface of LTO–LH electrode tested between 1 and 3 V after 3 cycles at rate of 0.1 C, but not on the LTO–LA electrode surface. In view of the fact that the electrolyte solution can only be reduced below 1 V, an SEI film was formed only on the LTO electrode surface when cycled between 0 and 3 V, not necessarily when cycled between 1 and 3 V. Therefore, the LTO–LH electrode presented quite different SEI film formation behavior from the LTO–LA electrode.

The simulation results given in Table 1 indicates that $R_{sei} = 62.3\ \Omega$ of LTO–LH obtained in the range of 1–3 V was much higher than the corresponding $R_{sei} = 2.4\ \Omega$ of LTO–LA, indicating the formation of a relatively thicker SEI film on the LTO–LH electrode. The total resistance ($R_b + R_{sei} + R_{ct} = 84.7\ \Omega$) of the cell made from LTO–LH measured after 3 cycles between 1 and 3 V was much higher than that using LTO–LA (35.4 Ω), proving that the poorer cyclic performance of LTO–LA between 1 and 3 V was not necessarily associated with the large polarization. However, it should be noted that both electrode materials had similarly excellent cyclic performance when cycled between 0 and 3 V at 1 C (Fig. S3). It is found previously that SEI films were normally formed on the LTO electrode surface due to the reduction of electrolyte solution (~0.7 V) [41]. It follows then that the surface chemistry and the properties of the SEI film affected the cyclic performance of the LTO–LA electrode.

To further evaluate the SEI film formation behaviors of the electrodes, SEM and TEM images of the electrode surface were taken after 3 and 160 charge/discharge cycles, as shown in Fig. 5 and Fig. S5. Judging from the fact that the electrolyte solution can only be reduced below 1 V (~0.7 V) [42], the SEI films formed on these electrodes cycled between 1 and 3 V (Fig. 5b–d) are not the reduction products of electrolyte solution, but rather a consequence from the intrinsic reaction between the LTO electrode and electrolyte solution, which often generates gases [43–45].

It is obvious that an SEI film was not formed on the LTO–LA electrode after the short 3 cycles (Fig. 5a) and the LTO–LA particles maintained the spinel structure (see the HRTEM image in Fig. S5a). Upon further cycling, the interfacial reaction occurred along with continuous release of gases. The interfacial reaction products were accumulated on the LTO–LA electrode to form an SEI film (Fig. 5b and Fig. S5b). A number of large pores were noted on the SEI film surface, which are assumed to have originated from the evaporation of gases from the reaction sites (Fig. 5b). Although the porous SEI film can suppress, to a certain extent, the reaction between the electrode and electrolyte, these pores also provide extra sites for gassing reactions between them. Through the above process, the electrolyte solution is gradually consumed with associated increases in resistance and polarization of the cells, deteriorating the cyclic performance of the electrode (Fig. 3a). However, a smooth and complete SEI film was formed on the LTO–LA electrode after short 3 cycles between 0 and 3 V due to the high rate reduction reaction of the electrolyte solution at ~0.7 V (Fig. S4a), which effectively separated the electrode from the surrounding electrolyte discouraging further reactions. It is seen from Fig. S4b that a

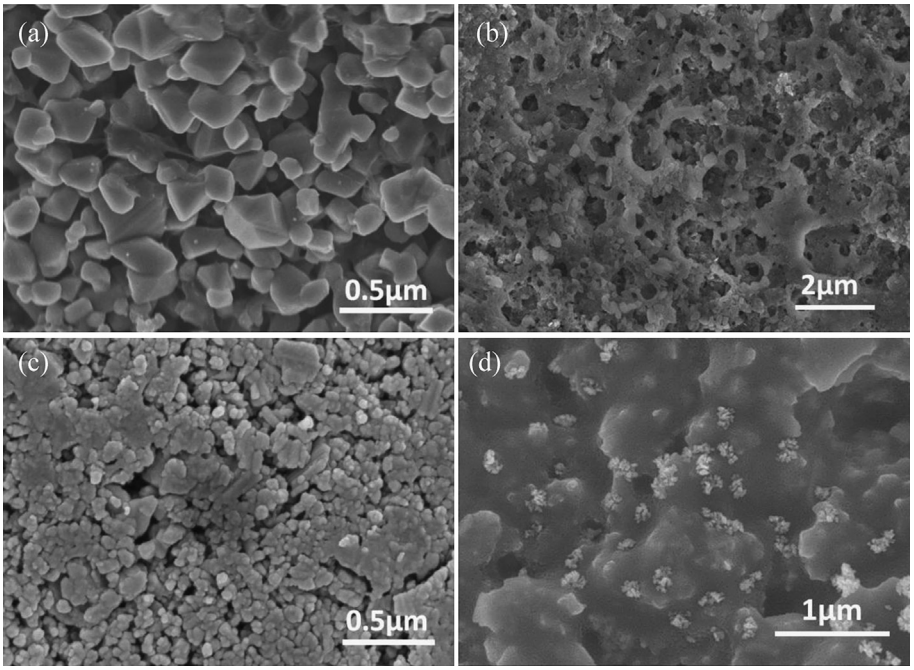


Fig. 5. SEM images of (a and b) LTO–LA and (c and d) LTO–LH electrodes obtained after 3 cycles at 0.1 C (a and c) and after 160 cycles according to Fig. 3a (b and d).

stable SEI film was retained on the LTO–LA electrode surface without any pores even after 160 cycles between 0 and 3 V, allowing excellent cyclic performance (Fig. S3).

When the two electrodes were cycled at a voltage range different from the above study, i.e. between 1 and 3 V, the formation behaviors of SEI films were also changed. For example, after 3 cycles an SEI film was formed on the LTO–LH electrode, and not on the LTO–LA electrode (Fig. 5a, c and Fig. S5a, c). This interesting observation appears to be associated with different morphologies and surface areas of the electrodes, which in turn determined the corresponding reactivity with the electrolyte. The LTO–LA powders with a cubic structure had a small surface area (0.41 $m^2\ g^{-1}$) and low reactivity with the electrolyte, and thus a complete SEI film was not formed after short 3 cycles (Fig. 5a). The small primary particles of LTO–LH powders with a much larger surface area (19.93 $m^2\ g^{-1}$) had high reactivity with the electrolyte, resulting in the formation of a smooth SEI film after 3 cycles (Fig. 5c and Fig. S5c). A thicker and stable SEI film was seen, which was built up on the LTO–LH electrode upon continued test to 160 cycles (Fig. 5d and Fig. S5d). The stable SEI film can separate the electrode from the surrounding electrolyte solution and suppress the interfacial reactions between them, which may explain the excellent cyclic performance of the LTO–LH electrode between 1 and 3 V (Fig. 3a).

To identify the different mechanisms of SEI film formation during cyclic tests between 0–3 V and 1–3 V, the XPS and FTIR were used to analyze the LTO–LH electrode surface at various stages, as shown in Fig. 6 and Fig. S6. Fig. 6a presents the Ti 2p detailed spectra: the neat LTO–LH powder gave a peak of Ti 2p3/2 at 458.6 eV and a peak of Ti 2p1/2 at 464.3 eV, which are in good agreement with Ti^{4+} ions in $Li_4Ti_5O_{12}$ [46]. After 160 cycles, these peaks totally disappeared (Fig. 6b, c), a reflection of the LTO particles covered by the SEI film as a reaction product of LTO and electrolyte solution. The O1s XPS profile presents a major peak at 532.8 eV assigned to C–O species, while three small peaks at 531.8, 532.4 and 533.8 eV are attributed to the Li_2CO_3, C=O species and the oxygen atom bonded with two carbon atoms in lithium alkyl carbonates (R–C–O–COOLi), respectively (Fig. 6e) [47,48]. The C1s detailed spectrum indicates that the species containing C–O group are the main reaction products of the SEI film (Fig. 6h). Fig. S6b presents the FTIR spectra of the LTO–LH electrode after 160 cycles between 1 and 3 V. In light of the comparison with the original LTO–LH electrode (Fig. S6a), an SEI layer composed of C–O species (at 1143, 1114, 1082 and 1043 cm^{-1}), Li_2CO_3 (at 866, 1425 and 1500 cm^{-1}) and $ROCO_2Li$ (at 1628 cm^{-1}) was formed [49,50]. It is seen that the C–O species are the main reaction products of the SEI film.

In sharp contrast, when the electrode was cycled between 0 and 3 V, the O1s and C1s XPS spectra gave different profiles, indicating that Li_2CO_3 and $ROCO_2Li$ were the main components of the SEI film (Fig. 6f and i), which is similar to the reaction product observed on the surface of graphite anode [51,52]. Moreover, the species containing C–O groups were also important components of the SEI film. These observations are consistent with the FTIR results (Fig. S6c). The different chemistries of the SEI films between the electrodes cycled in the two different voltage ranges mean that their formation mechanisms were also different. It is interesting to note that the electrolyte solution was reduced to form Li_2CO_3 and $ROCO_2Li$ species (when cycled between 0 and 3 V), whereas the species containing C–O groups as the main components of the SEI film (when cycled between 1 and 3 V) were not associated with the reduction of electrolyte. The gases generated in LTO-based batteries are H_2, CO_2 and CO [44,45], and the C–O species may be attributed to the interfacial decarboxylation reaction between LTO and the electrolyte [45].

As an effective solution to prevent the formation of detrimental pores on the SEI film of the LTO–LA electrode, vinylene carbonate (VC) was used as an additive with a reduction potential of 1.5 V in the electrolyte solution [29,53]. When 2 wt.% VC (1 M $LiPF_6$/EC + DMC + EMC + 2 wt.% VC) was added in the electrolyte, it facilitated the formation a barrier SEI film on the electrode which in turn separated the electrode from the electrolyte solution and thus suppressed the interfacial reactions between them, see SEM image shown in Fig. 7a. Fig. 7b clearly indicates that the additive had an

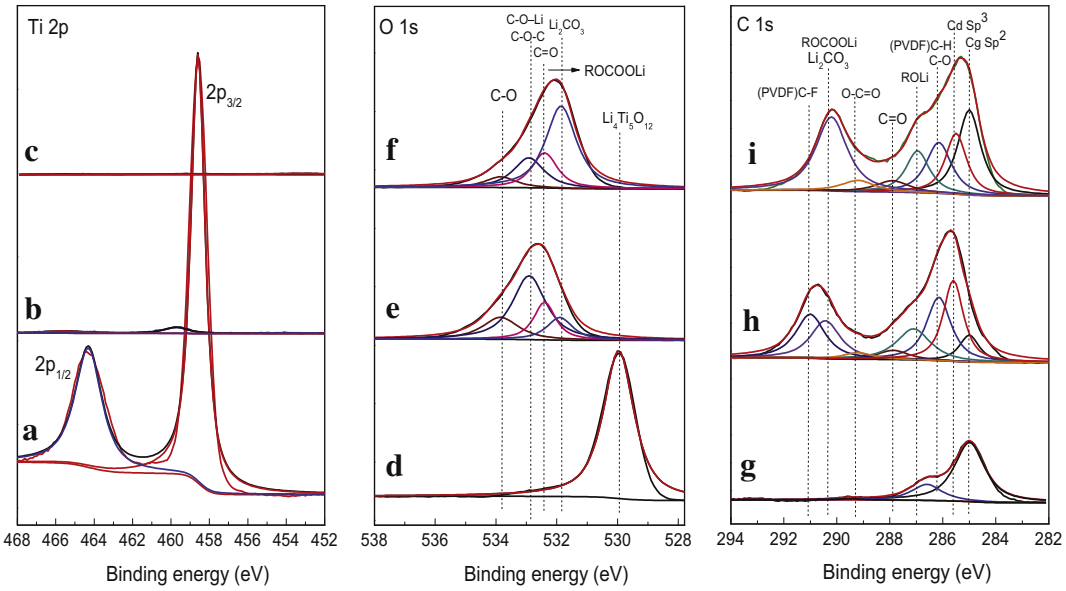


Fig. 6. Ti 2p, O 1s and C 1s XPS detailed spectra of LTO–LH electrode under different conditions: (a, d, g) as-prepared LTO–LH powder; LTO–LH electrode after 160 cycles (b, e, h) between 1 and 3 V and (c, f, i) between 0 and 3 V. Note that the LTO–LH electrodes were fully charged before XPS examinations.

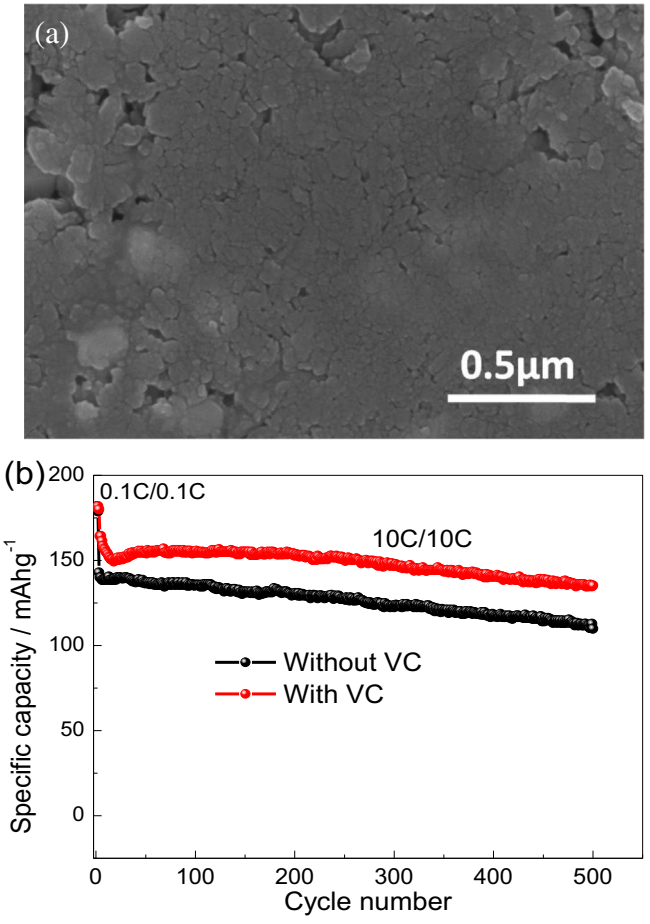


Fig. 7. Effects of VC on the performance of LTO–LA electrode: (a) SEM image of LTO–LA electrode using electrolyte with VC after 3 cycles at 0.1 C between 1 and 3 V; (b) cyclic performance of LTO–LA using electrolyte with and without VC.

ameliorating effect of improving the cyclic performance of the LTO–LA electrode: it delivered a stable specific capacity of 155.6 mAh g^{-1} at 10 C and retained a remarkable value of 135.2 mAh g^{-1} even after 500 cycles. These achievements are well above the corresponding values of the electrode without VC: namely, a stable capacity of 139.5 mAh g^{-1} and a capacity of 109.9 mAh g^{-1} measured after 500 cycles.

4. Conclusion

$Li_4Ti_5O_{12}$ (LTO) anode powders with different morphologies are synthesized using lithium acetate (LA) and lithium hydroxide (LH) as the lithium sources based on a hydrothermal method to study the formation mechanisms of SEI films. Both the LTO–LA and LTO–LH anodes present excellent rate performance with specific capacities of 139.7 and 144.9 mAh g^{-1}, respectively, at a high charge/discharge rate of 10 C. These two anodes have largely dissimilar interfacial reactions with the electrolyte solution and formation characteristics of SEI films. The LTO–LH powders consist of agglomerates of irregularly-shaped primary nanoparticles with a large surface area and have high reactivity with the electrolyte to form a smooth SEI film within a few cycles. In contrast, the LTO–LA powders with a cubic structure and a small surface area tend to form a porous SEI film only after long cycles, say 160 cycles. The different powder morphologies and SEI film characteristics result in slightly lower cyclic performance of the LTO–LA anode than the LTO–LH anode when cycled between 1 and 3 V. A barrier SEI film is formed on the LTO–LA anode surface when an electrolyte additive like vinylene carbonate (VC) is added, which in turn greatly improves the high rate and cyclic performance of the electrode.

Acknowledgments

This project was supported by the Research Grants Council (GRF Projects: 613811 and 613612) of Hong Kong SAR. The authors appreciate the technical assistance from the Materials Characterization and Preparation Facilities (MCPF) of HKUST.

Appendix A. Supplementary data

Supplementary data related to this article can be found online at http://dx.doi.org/10.1016/j.jpowsour.2013.03.141.

References

[1] E. Ferg, R.J. Gummow, A.d. Kock, M.M. Thackeray, J. Electrochem. Soc. 141 (1994) L147–L150.
[2] T. Ohzuku, A. Ueda, N. Yamamoto, J. Electrochem. Soc. 142 (1995) 1431–1435.
[3] L. Aldon, P. Kubiak, M. Womes, J.C. Jumas, J. Olivier-Fourcade, J.L. Tirado, J.I. Corredor, C.P. Vicente, Chem. Mater. 16 (2004) 5721–5725.
[4] Y.-Q. Wang, L. Gu, Y.-G. Guo, H. Li, X.-Q. He, S. Tsukimoto, Y. Ikuhara, L.-J. Wan, J. Am. Chem. Soc. 134 (2012) 7874–7879.
[5] L. Zhao, Y.S. Hu, H. Li, Z.X. Wang, L.Q. Chen, Adv. Mater. 23 (2011) 1385–1388.
[6] G.J. Wang, J. Gao, L.J. Fu, N.H. Zhao, Y.P. Wu, T. Takamura, J. Power Sources 174 (2007) 1109–1112.
[7] G.-N. Zhu, H.-J. Liu, J.-H. Zhuang, C.-X. Wang, Y.-G. Wang, Y.-Y. Xia, Energy Environ. Sci. 4 (2011) 4016–4022.
[8] B. Li, C. Han, Y.B. He, C. Yang, H. Du, Q.H. Yang, F. Kang, Energy Environ. Sci. 5 (2012) 9595–9602.
[9] H.G. Jung, S.T. Myung, C.S. Yoon, S.B. Son, K.H. Oh, K. Amine, B. Scrosati, Y.K. Sun, Energy Environ. Sci. 4 (2011) 1345–1351.
[10] K.S. Park, A. Benayad, D.J. Kang, S.G. Doo, J. Am. Chem. Soc. 130 (2008) 14930–14931.
[11] S.Z. Ji, J.Y. Zhang, W.W. Wang, Y. Huang, Z.R. Feng, Z.T. Zhang, Z.L. Tang, Mater. Chem. Phys. 123 (2010) 510–515.
[12] B. Tian, H. Xiang, L. Zhang, Z. Li, H. Wang, Electrochim. Acta 55 (2010) 5453–5458.
[13] B. Zhang, Z.D. Huang, S.W. Oh, J.K. Kim, J. Power Sources 196 (2011) 10692–10697.
[14] S.H. Huang, Z.Y. Wen, X.J. Zhu, Z.H. Gu, Electrochem. Commun. 6 (2004) 1093–1097.
[15] X. Li, M.Z. Qu, Y.J. Huai, Z.L. Yu, Electrochim. Acta 55 (2010) 2978–2982.
[16] X. Li, M.Z. Qu, Z.L. Yu, Solid State Ionics 181 (2010) 635–639.
[17] R. Cai, X. Yu, X. Liu, Z. Shao, J. Power Sources 195 (2010) 8244–8250.
[18] B. Zhang, Y.S. Liu, Z.D. Huang, S. Oh, Y. Yu, Y.W. Mai, J.K. Kim, J. Mater. Chem. 22 (2012) 12133–12140.
[19] B. Zhang, Y. Yu, Y. Liu, Z.D. Huang, Y.B. He, J.K. Kim, Nanoscale 5 (2013) 2100–2106.
[20] W.J.H. Borghols, M. Wagemaker, U. Lafont, E.M. Kelder, F.M. Mulder, J. Am. Chem. Soc. 131 (2009) 17786–17792.
[21] Y. Tang, L. Yang, S. Fang, Z. Qiu, Electrochim. Acta 54 (2009) 6244–6249.
[22] Y.F. Tang, L. Yang, Z. Qiu, J.S. Huang, Electrochem. Commun. 10 (2008) 1513–1516.
[23] J. Chen, L. Yang, S. Fang, Y. Tang, Electrochim. Acta 55 (2010) 6596–6600.
[24] C. Lai, Y.Y. Dou, X. Li, X.P. Gao, J. Power Sources 195 (2010) 3676–3679.
[25] S.S. Zhang, K. Xu, T.R. Jow, J. Power Sources 130 (2004) 281–285.
[26] H. Schranzhofer, J. Bugajski, H.J. Santner, C. Korepp, K.C. Moller, J.O. Besenhard, M. Winter, W. Sitte, J. Power Sources 153 (2006) 391–395.
[27] S.S. Zhang, K. Xu, T.R. Jow, Electrochim. Acta 51 (2006) 1636–1640.
[28] M. Herstedt, H. Rensmo, H. Siegbahn, K. Edström, Electrochim. Acta 49 (2004) 2351–2359.
[29] H.H. Lee, Y.Y. Wang, C.C. Wan, M.H. Yang, H.C. Wu, D.T. Shieh, J. Appl. Electrochem. 35 (2005) 615–623.
[30] Y.B. He, Z.Y. Tang, Q.S. Song, H. Xie, Y.G. Liu, Q. Xu, J. Electrochem. Soc. 155 (2008) A481–A487.
[31] Y.B. He, B.H. Li, Q.H. Yang, H.D. Du, F. Kang, G.W. Ling, Z.Y. Tang, J. Solid State Electrochem. 15 (2011) 1977–1985.
[32] S.B. Lee, S.-I. Pyun, Carbon 40 (2002) 2333–2339.
[33] H.H. Lee, Y.Y. Wang, C.C. Wan, M.H. Yang, H.C. Wu, D.T. Shieh, J. Power Sources 134 (2004) 118–123.
[34] R. Spotnitz, J. Franklin, J. Power Sources 113 (2003) 81–100.
[35] N.A. Kaskhedikar, J. Maier, Adv. Mater. 21 (2009) 2664–2680.
[36] C. Liu, F. Li, L.P. Ma, H.M. Cheng, Adv. Mater. 22 (2010) E28–E62.
[37] F. Nobili, R. Tossici, F. Croce, B. Scrosati, R. Marassi, J. Power Sources 94 (2001) 238–241.
[38] F. Croce, F. Nobili, A. Deptula, W. Lada, R. Tossici, A. D'Epifanio, B. Scrosati, R. Marassi, Electrochem. Commun. 1 (1999) 605–608.
[39] M. Umeda, K. Dokko, Y. Fujita, M. Mohamedi, I. Uchida, J.R. Selman, Electrochim. Acta 47 (2001) 885–890.
[40] G.T.K. Fey, W.H. Yo, Y.C. Chang, J. Power Sources 105 (2002) 82–86.
[41] J. Shu, Electrochem. Solid State Lett. 11 (2008) A238–A240.
[42] Y.B. He, F. Ning, B.H. Li, Q.S. Song, W. Lv, H.D. Du, D.Y. Zhai, F.Y. Su, Q.H. Yang, F. Kang, J. Power Sources 202 (2012) 253–261.
[43] M. Kitta, T. Akita, Y. Maeda, M. Kohyama, Langmuir 28 (2012) 12384–12392.
[44] I. Belharouak, G.M. Koenig Jr., T. Tan, H. Yumoto, N. Ota, K. Amine, J. Electrochem. Soc. 8 (2012) A1165–A1170.
[45] Y.B. He, B. Li, M. Liu, C. Zhang, W. Lv, C. Yang, J. Li, H. Du, B. Zhang, Q.H. Yang, J.K. Kim, F. Kang, Sci. Rep. 2 (2012) 913.
[46] R. Dedryvere, D. Foix, S. Franger, S. Patoux, L. Daniel, D. Gonbeau, J. Phys. Chem. C 114 (2010) 10999–11008.
[47] M. Herstedt, A.M. Andersson, H. Rensmo, H. Siegbahn, K. Edstrom, Electrochim. Acta 49 (2004) 4939–4947.
[48] R. Dedryvere, L. Gireaud, S. Grugeon, S. Laruelle, J.M. Tarascon, D. Gonbeau, J. Phys. Chem. B 109 (2005) 15868–15875.
[49] X.W. Guo, X.P. Fang, Y. Sun, L.Y. Shen, Z.X. Wang, L.Q. Chen, J. Power Sources 226 (2013) 75–81.
[50] J. Shu, M.A. Shui, F.T. Huang, D. Xu, Y.L. Ren, L. Hou, J. Cui, J.J. Xu, J. Phys. Chem. C 115 (2011) 6954–6960.
[51] C.R. Yang, Y.Y. Wang, C.C. Wan, J. Power Sources 72 (1998) 66–70.
[52] R. Dedryvère, H. Martinez, S. Leroy, D. Lemordant, F. Bonhomme, P. Biensan, D. Gonbeau, J. Power Sources 174 (2007) 462–468.
[53] S.S. Zhang, J. Power Sources 162 (2006) 1379–1394.